TOPOLOGICAL REPRESENTATION OF THE POROUS STRUCTURE AND ITS EVOLUTION OF RESERVOIR SANDSTONE UNDER EXCAVATION-INDUCED LOADS

by

Yang JU[a,b*], Yongming YANG[c], Xi ZHAO[c], Feng GAO[a], Wei SONG[d], and Jianguo WANG[a]

[a] State Key Laboratory for Geomechanics and Deep Underground Engineering, China University of Mining and Technology, Xuzhou, China
[b] State Key Laboratory of Coal Resources and Safe Mining, China University of Mining and Technology, Beijing, China
[c] School of Mechanics and Civil Engineering, China University of Mining and Technology Beijing, Beijing, China
[d] Refinery of Shandong Gold Mining Co., Ltd, Laizhou, China

Original scientific paper
https://doi.org/10.2298/TSCI17S1285J

The porous structure of a reservoir rock greatly influences its evolutive deformation and fracture behavior during excavation of natural resources reservoirs. Most numerical models for porous structures have been used to predict the quasi-static mechanical properties, but few are available to accurately characterize the evolution process of the porous structure and its influence on the macroscopic properties of reservoir rocks. This study reports a novel method to characterize the porous structure of sandstone using its topological parameters and to determine the laws that govern the evolutive deformation and failure of the topological structure under various uniaxial compressive loads. A numerical model of the porous sandstone was established based on the pore characteristics that were acquired using computed tomography imaging techniques. The analytical method that integrates the grassfire algorithm and the maximum inscribed sphere algorithm was proposed to create the 3-D topological model of the deformed porous structure, through which the topological parameters of the structure were measured and identified. The evolution processes of the porous structure under various loads were characterized using its equivalent topological model and parameters. This study opens a new way to characterize the dynamic evolution of the pore structure of reservoir sandstone under excavation disturbance.

Key words: *porous structure, topological representation, reservoir sandstone, deformation and fracture, numerical characterization*

Introduction

The deformation and fracture of a reservoir rock is a dynamic process induced by underground oil and gas resource excavation and recovery in the presence of a complex in-situ stress field. The initial equilibrium stress field of reservoir rock is perturbed and the structure of the rock continuously deforms to fracture during excavation processes [1, 2]. Reservoir rock contains pores of various sizes, which provide storage space and transport channels for oil and

* Corresponding author, e-mail: juy@cumtb.edu.cn

gas resources, and the skeleton of the rock supports external loads [3-5]. The evolutive deformation and fracture of the pore structure significantly affect the rock's physical and mechanical properties, including deformability, strength, permeability, storage capacity, and transport properties [6, 7]. Therefore, understanding and quantitative characterization of the evolution of pore structures of rocks induced by reservoir excavation is of great significance for accurately evaluating the production and recovery of oil and gas resources.

However, the large number and irregular spatial distribution of the pores make it extremely difficult to analytically describe the evolution of the porous structure in response to complex excavation stresses. Alternatively, field tests, laboratory experiments and numerical models are commonly used to analyze the physical and mechanical properties of porous rock. In field tests, as oil and gas reservoirs are usually buried thousands of meters beneath the Earth's surface, the size of the pores that affect the rock's properties and ability to store and transport oil and gas is usually on the order of millimeters or smaller [8, 9], it is extremely hard to detect variations of the porous structure on this scale using the available detection technology. In laboratory tests, the development of computed tomography (CT) imaging [10, 11], scanning electron microscopy (SEM) [12], nuclear magnetic resonance (NMR) [13] and the other advanced imaging technologies have made it possible to observe the microstructures of porous media. However, the evolution of the structure of porous rock during excavation is a dynamic process due to variation of external loads and other conditions. To date, it is still difficult to incorporate loading equipment and imaging devices to observe real-time variations of the porous structures of rocks.

Considering the limitations of field and laboratory tests, researchers have attempted to adopt numerical models to analyze microscopic porous structures. With improvements in computational methods, a few digital core construction methods have been developed [14-16], these include the Gaussian field method, process simulation algorithms, and simulated annealing methods [17-21]. These digital core models represent the geometrical features of the porous structure and can be used to determine the macroscopic properties based on a description of the pore structure. One of the most representative models commonly used to simulate porous media is known as the pore network model [22]. In these models, the apparent transport properties of reservoir rock can be observed, but few are available for elucidating the effective law relating the evolution of the pore structure and the observable macroscopic properties of the rock.

To quantitatively characterize the porous structure and the influence of its evolution on the macroscopic properties of reservoir rocks, topological parameters of the porous structure, such as the pore radius, throat radius and coordination number are often used [23-26]. Despite of present achievements, it is noteworthy that most numerical models of pore structures are able to predict the static or quasi-static physical and mechanical properties that relate to the porous structure, but few can accurately characterize the dynamic evolution of the porous structure and its influence on the macroscopic mechanical behavior of rocks.

We intend to construct a topological model of a reservoir rock to characterize the porous structure and its dynamic evolution using the topological features and to determine the laws that govern the evolution of the deformed topology as a result of excavation-induced loads. The topological skeleton was used to create the 3-D network model, based on which the 3-D topological parameters of the deformed porous structure, such as pore, throat, and co-ordination numbers, pore and throat radii, pore-to-throat ratios, were identified and measured. The dynamic evolution processes including deformation and fracture of the pore structure characterized using the topological features induced by external loads were elucidated thoroughly.

Constructing the porous sandstone model

A micro focus CT system with a spacial resolution up to 4 μm was employed to identify the morphology of pore structures. The reservoir sandstone samples for the CT test have a low matrix granularity and scale 25 mm in diameter and 50 mm in height. Each sample was scanned from top end to bottom end with a voxel size of 25 μm. Figure 1(a) demonstrates one of the 2-D CT slices with a precision of 1024 × 1024 pixels. To distinguish the pores from the matrix, the CT images were binarized into the two-phase images that only comprise the pixels of pores and matrices. In the process, the gray values of matrix and pore pixels were set to be 255 and 0. To attain the accurate and complete geometrical and distribution characteristics of pores, the median filtering and multi-threshold segmentation methods [27-29] were adopted to remove the noisy points and identify the pores using the self-developed computer program. Figure1(b) shows a binarized 2-D image of pores on the selected cross-section of the rock sample. According to the binarized CT image, it is shown that the porosity of the sandstone is approximately 15% and the probability density of the equivalent pore radius complies with exponential distribution law [30] which is in good agreement with the pore radius distribution of the nature sandstone. After processing, the binarized CT images were imported to the softwares MIMICS® (http://materialise.com/) and ANSYS® (http://www.ansys.com/) to generate the 3-D model of the porous sandstone. A total of 200 square slices with a precision of 200 × 200 pixels were inscribed out of the 2-D circular binarized CT images of the representative layers to form the cubic model with side lengths of 5 mm, as shown in fig. 2.

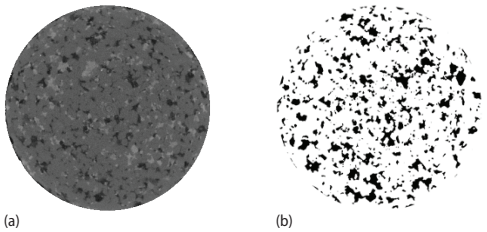

Figure 1. The CT image processing; (a) the original CT scanning image, (b) the binarized CT image by applying median filtering and threshold segmentation

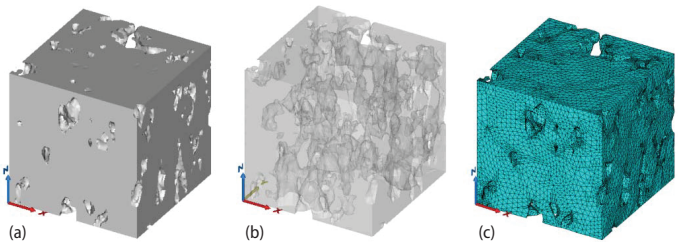

Figure 2. The constructed cubic porous sandstone model; (a) the matrix of the model, (b) the perspective drawing of the model, and (c) finite element meshes of the model

Measurement of topological characteristics of deformed porous structures subjected to loading

Construction of finite element model

To probe the deformation and failure behavior of the porous sandstone subjected to loads, we carried out the numerical simulation compressive tests based on the porous sandstone. Table 1 lists the mechanical properties of the sandstone that were attained from the laboratory tests [7, 31]. These material parameters were assigned to elements according to the grey values of the element pixels.

Boundary conditions and failure criteria

To study the effect of external loads on the deformation and fracture of the porous rock, the following boundary conditions were applied to the numerical model: at the bottom of

Table 1 Mechanical properties of the tested sandstone

Elastic modulus E [GPa]	Poissons ratio μ	Cohesion C [MPa]	Internal friction angle ϕ [°]	Compressive strength σ_c [MPa]	Tensile strength σ_t [MPa]
42.6	0.23	21.94	30	67.89	12.59

the model (*i. e.* x-y plane with $z = 0$) constraints were applied to all displacement directions, on the top plane of the model the uniaxial compression stress was continuously applied in six steps from 10 MPa, 20 MPa, 30 MPa, 40 MPa, 50 MPa, and 60 MPa, and to take into account the effect of underground *in-situ* geostresses. The confining stress 10 MPa was applied on the other four surfaces of the model.

Three different failure criteria, *i. e.* the Drucker-Prager criterion, the maximum compressive stress criterion, and the ultimate tensile stress criterion, were set to the threshold condition of element failure. The element will be perished whichever criterion is satisfied first.

Methodology

This part explains the methods that were used to measure the topological characteristics and construct the topological model of the deformed porous structure of sandstone subjected to various compressive loads. The method that integrates the Blum's grassfire algorithm and the maximum inscribed sphere algorithm is proposed to construct an equivalent topological skeleton of a porous structure. The 3-D topological characteristics and the evolution of the deformed porous structure under various loads are identified and analyzed based on the aforementioned numerical simulation results.

To achieve the goal, we adopted the Blum's grassfire algorithm [32] and the maximum inscribed sphere algorithm [33] together to create a skeleton model that is topologically equivalent to the porous system. In fig. 3(a), the red lines envelop the fire areas, and the red arrows indicate the moving direction of fire. The yellow line represents the medial axis. Let us assume a 2-D porous structure, see fig. 3(b), for instance, in which the white lattices constitute the pore space and the gray lattices make up the solid matrix. Applying the grassfire algorithm along with the 8-connectivity approach (*i. e.* each point of interest connects with the eight neighboring points) to the 2-D porous structure generates the skeleton represented by large numbers, where the numbers marked in lattices indicate burning steps. If the 4-connectivity approach is applied, the red lattices will be burned up in Step # 2 rather than in Step # 1 as the result of applying 8-connectivity approach. For a 3-D system, the 26-connectivity approach may apply, in which 26 neighboring voxels of the voxel of interest are taken into account.

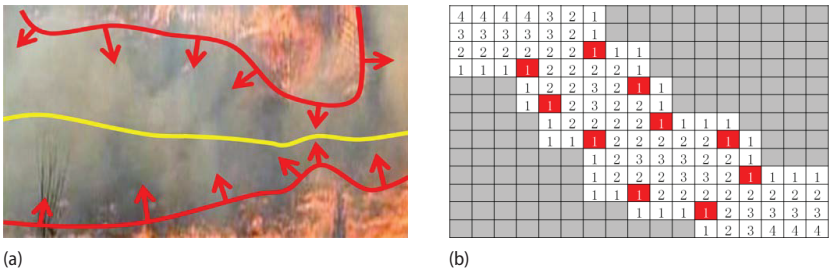

Figure 3. Illustration of the Blum's grassfire algorithm for determining the required skeleton; (a) basic principle of the algorithm and (b) the extraction of a skeleton from the 2-D porous structure using the 8-adjacency rule and 4-adjacency rule (*for color image see journal web site*)

A dilation algorithm was performed to find the radii of pores and throats. The measuring procedure starts from the media axis voxel and creates a sphere with a radius of one voxel and check if there is any overlap between the inscribed sphere and the surrounding matrix. If there is an overlap, the procedure stops and the obtained radius is considered as the radius of the pore. If there is no overlap, the algorithm proceeds by increasing the radius by one voxel, and repeats the previous step until an overlap between the matrix and sphere occurs. In some cases, two and more voxels occupation can be considered as one void space; a merging criterion is adopted in which two inscribed pore bodies are merged if they overlap and the largest inscribed pore body is chosen to be the inscribed pore [33]. Figure 4 shows the merging of two inscribed pores that occupy the same void space and the methods that were used to define the largest inscribed pore radii and the smallest inscribed throat radii. The same dilation algorithm was used to determine the throat radii. The inscribed throat is located at the voxel with the minimum burning number along the medial axis connecting two neighboring voxels. The approach can find its origin in [33].

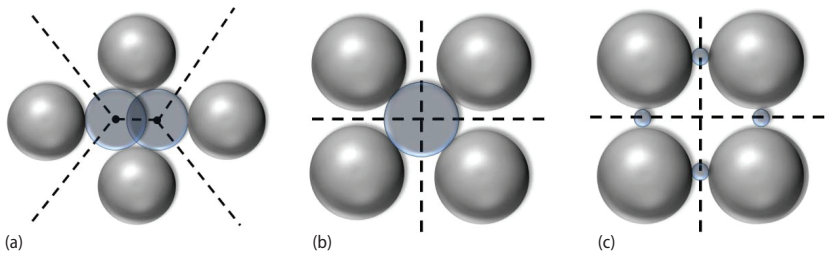

Figure 4. Diagram of defining the radii of inscribed pores and throats

Measurement and analysis of the topological parameters of the deformed porous structures

The previous methods were applied to measuring the topological parameters of the deformed structures under various external loads. The simulation results embody the effects of deformation and fracture of matrix skeleton under various loads, which modify the topological parameters of the porous structures. The 3-D topological parameters were measured based on these deformed porous structures. A MATLAB based program was developed to automatically measure the 3-D topological parameters of the deformed porous structures. Table 2 lists the extraction results of the parameters. Figure 5 presents the equivalent topological network model of the deformed structures using these parameters, in which the red and the green spheres rep-

Table 2. The 3-D topological parameters of the deformed structures under various compressive loads

Loads	Pore number	Throat number	Average co-ordination number	Pore radius (voxel)	Throat radius (voxel)	Pore-to--throat ratio
10 MPa	388	755	4.0521	6.9240	5.7782	1.1983
20 MPa	405	765	4.0523	7.2181	6.0924	1.1848
30 MPa	420	787	4.0541	7.3663	6.2522	1.1782
40 MPa	446	790	4.0595	7.4822	6.3782	1.1731
50 MPa	531	890	4.0764	7.5020	6.3996	1.1723
60 MPa	696	1171	4.1084	8.1892	7.1654	1.1429

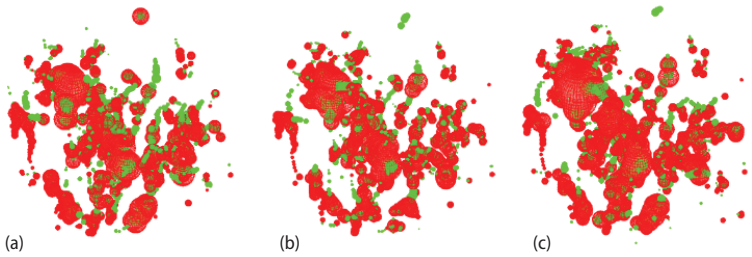

Figure 5. The 3-D equivalent topological network models of the deformed structures under compressive loads 10 MPa, 30 MPa, and 50 MPa using the measured parameters, in which the red and the green spheres represent the pores and throats, respectively
(*for color image see journal web site*)

resent the pores and throats, respectively. Figure 6 shows the variations in the 3-D topological parameters as the external load increases.

These measurement results indicate that the numbers of pores and throats vary little as the uniaxial compressive load rises from 10 MPa to 50 MPa but increase apparently once the load jumps over 50 MPa. This implies that the porous structure has not been destructed severely before the compressive load exceeds 50 MPa. Once the load is beyond this threshold value, the number of failed elements dramatically increases, resulting in the apparent increases in the pore and throat numbers. The average co-ordination number and the average radii of pores and throats shows a similar increasing tendency, *i. e.* the average co-ordination number and the average radii ascend gradually before the compressive load reaches 50 MPa and the parameters ascend abruptly once the load exceeds the threshold 50 MPa. Elevating compressive loads aggravates failure of the porous structure and increases the connectivity of porous structures.

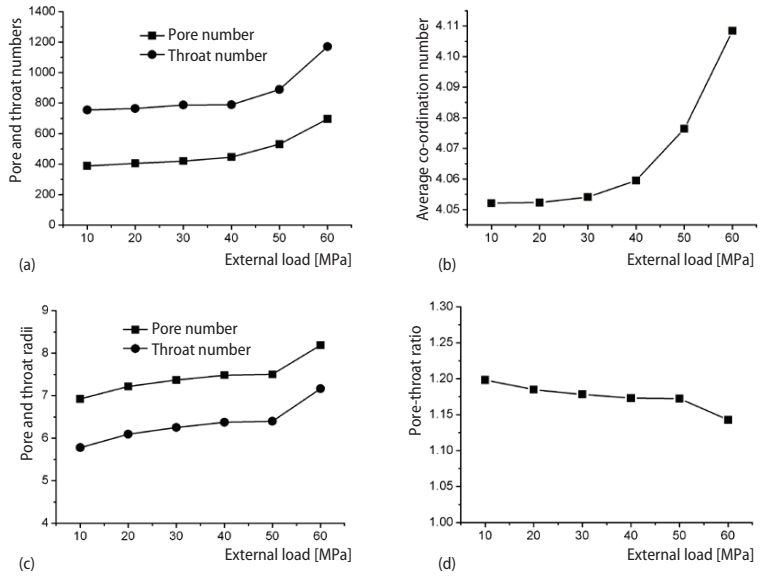

Figure 6. Variation in the 3-D topological parameters changing with the external load; (a) pore and throat numbers, (b) average co-ordination numbers, (c) pore and throat radii, and (d) pore-to-throat ratios

In contrast, the pore-to-throat ratio gradually decreases as the load increases, which means that the increment of throat radii is larger than that of pore radii. It implies that the failure occurs preferentially in the smaller pore regions of the porous structure.

Conclusions

The stress disturbance induced by underground resources excavation greatly influences the dynamic evolution of the porous structure and then the deformation and failure performance of reservoir rock. This paper reports a novel method to characterize the porous structure of reservoir sandstone using its topological parameters and to analyze the deformation and failure behavior of the topological structure as a result of excavation-induced loads. The deformation and fracture of the pore structure under various loads was numerically analyzed based on its numerical model that was established by means of the finite element method and the CT imaging technique. The grassfire algorithm and the maximum inscribed sphere algorithm was adopted to create the 3-D equivalent topological model of the deformed porous structure, through which the topological parameters of the deformed pore structure, such as pore number, throat number, co-ordination number, pore radius, throat radius and pore-to-throat ratio, were measured and identified. The evolution of the deformed porous structure under various loads was characterized using its equivalent topological model and parameters.

The analysis indicates that there is a threshold value for the applied uniaxial compressive load over which the number of pores and throats, the average co-ordination number, the average radii of pores and throats will apparently increase with the increment of the external loads. Elevating compressive loads aggravates failure of the matrix skeleton and then increases the connectivity of the porous structures. In contrast, the pore-to-throat ratio gradually decreases as the load increases, which means that the failure occurs preferentially in the smaller pore regions of the porous structure.

Acknowledgment

The authors gratefully acknowledge financial support from the State Key Research Development Program of China (Grant No. 2016YFC0600705), the National Natural Science Foundation of China (Grants No. 51374213, 51674251), the National Natural Science Fund for Distinguished Young Scholars of China (Grant No. 51125017), Fund for Innovative Research and Development Group Program of Jiangsu Province (Grant No. 2014-27), and the Priority Academic Program Development of Jiangsu Higher Education Institutions (Grant No. PAPD 2014).

References

[1] Fahimifar, A., *et al.*, Analytical Solution for the Excavation of Circular Tunnels in a Viscoelastic Burger's Material under Hydrostatic Stress Field, *Tunn. Undergr. Sp. Tech.*, *25* (2010), 4, pp. 297-304
[2] Stiros, S. C., Kontogianni, V. A., Coulomb Stress Changes: from Earthquakes to Underground Excavation Failures, *Int. J. Rock Mech. Min.*, *46* (2009), 1, pp. 182-187
[3] Cueto, N., *et al.*, Rock Fabric, Pore Geometry and Mineralogy Effects on Water Transport in Fractured Dolostones, *Eng. Geol.*, *107* (2009), 1-2, pp. 1-15
[4] Sabatakakis, N., *et al.*, Index Properties and Strength Variation Controlled by Microstructure for Sedimentary Rocks, *Eng. Geol.*, *97* (2008), 1-2, pp. 80-90
[5] Zaretskiy, Y., *et al.*, Efficient Flow and Transport Simulations in Reconstructed 3D Pore Geometries, *Adv. Water Resour.*, *33* (2010), 12, pp. 1508-1516
[6] Varloteaux, C., *et al.*, Pore Network Modelling to Determine the Transport Properties in Presence of a Reactive Fluid: From Pore to Reservoir Scale, *Adv. Water Resour.*, *53* (2013), 2, pp. 87- 100
[7] Bultreys, T., *et al.*, Multi-Scale, Micro-Computed Tomography-Based Pore Network Models to Simulate Drainage in Heterogeneous Rocks, *Adv. Water Resour.*, *78* (2015), Apr., pp. 36-49

[8] Kate, J. M., Gokhale, C. S., A Simple Method to Estimate Complete Pore Size Distribution of Rocks, *Eng. Geol.*, *84* (2006), 1-2, pp. 48-69
[9] Bera, B., *et al.*, Understanding the Micro Structure of Berea Sandstone by the Simultaneous Use of Micro-Computed Tomography (Micro-CT) and Focused Ion Beam-Scanning Electron Microscopy (FIB-SEM), *Micron*, *42* (2011), 5, pp. 412-418
[10] De Boever, W., *et al.*, Data-Fusion of High Resolution X-Ray CT, SEM and EDS for 3D and Pseudo-3D Chemical and Structural Characterization of Sandstone, *Micron*, *74* (2015), July, pp. 15- 21
[11] Omer, M. F., Cathodoluminescence Petrography for Provenance Studies of the Sandstones of Ora Formation (Devonian–Carboniferous), Iraqi Kurdistan Region, Northern Iraq, *Journal of African Earth Sciences*, *109* (2015), Sept., pp. 195-210
[12] Rosenbrand, E., *et al.*, Permeability in Rotliegend Gas Sandstones to Gas and Brine as Predicted from NMR, Mercury Injection and Image Analysis, *Marine & Petroleum Geology*, *64* (2015), June, pp.189-202
[13] Liu, X. F., *et al.*, Numerical Simulation of Rock Electrical Properties Based on Digital Cores, *J. Appl. Geophys.*, *6* (2009), 1, pp. 1-7
[14] Luo, G., Wang, L. 3D Morphology Algorithm Implementation and Application, in: *High Quality Artificial Digital Core Modeling* (Ed. Z. Qian *et al.*), Springer, Heidelberg, Berlin, 2012, pp. 817-822
[15] Zhu, W., *et al.*, Digital Core Modeling from Irregular Grains, *J. Appl. Geophys.*, *85* (2012), 10, pp. 37-42
[16] Bakke, S., Ren, P. E., 3-D Pore-Scale Modelling of Sandstones and Flow Simulations in the Pore Networks, *SPE*, *2* (1997), 2, pp. 136-149
[17] Hazlett, R. D., Statistical Characterization and Stochastic Modeling of Pore Networks in Relation to Fluid Flow, *Mathematical Geology*, *29* (1997), 6, pp. 801-822
[18] Ren, P. E., Bakke, S., Process Based Reconstruction of Sandstones and Prediction of Transport Properties, *Trans Porous Med.*, *46* (2002), 2-3, pp. 311-343
[19] Quiblier, J. A., A New Three-Dimensional Modeling Technique for Studying Porous Media, *J. Colloid Interf. Sci.*, *98* (1984), 1, pp. 84-102
[20] Yeong, C. L. Y., Torquato, S., Reconstructing Random Media. II. Three-Dimensional Media from Two-Dimensional Cuts, *Phys. Rev. E*, *Statistical Physics Plasmas Fluids & Related Interdisciplinary Topics*, *58* (1998), 1, pp. 224-233
[21] Blunt, M. J., *et al.*, Pore-Scale Imaging and Modelling, *Adv. Water Resour.*, *51* (2013), 1, pp. 197-216
[22] Ju, Y., *et al.*, 3D Numerical Reconstruction of Well-Connected Porous Structure of Rock Using Fractal Algorithms, *Comput. Methods Appl. Mech. Eng.*, *279* (2014), 9, pp. 212-226
[23] Knackstedt, M. A., *et al.*, Pore Network Modelling of Two-Phase Flow in Porous Rock: The Effect of Correlated Heterogeneity, *Adv. Water Resour.*, *24* (2001), 3-4, pp. 257-277
[24] Su, N., Study of Effects of Pore Space Topological Structure on Water-Oil Two Phase Flow (in Chinese), *Journal of Chongqing University of Science & Technology,* (2013), 3, pp. 52-58
[25] Valvatne, P. H., *et al.*, Predictive Pore-Scale Modeling of Single and Multiphase Flow, *Transport Porous Med.*, *58* (2005), 1-2, pp. 23-41
[26] Ju, Y., *et al.*, Computer Program for Extracting and Analyzing Fractures in Rocks and Concretes (in Chinese), Software Copyright Registration, Reg # 0530646, Beijing, 2013
[27] Kaestner, A., *et al.*, Imaging and Image Processing in Porous Media Research, *Adv. Water Resour.*, *31* (2008), 9, pp. 1174-1187
[28] Otsu, N., A Threshold Selection Method from Gray-Level Histograms, *IEEE Transactions on Systems Man & Cybernetics*, *9* (1979), 1, pp. 62-66
[29] Ju, Y., *et al.*, A Statistical Model for Porous Structure of Rocks, *Sci. China Technol. Sc.*, *51* (2008), 11, pp. 2040-2058
[30] Wang, J. B., 3D Reconstruction of Porous Rock and Numerical Simulations of Fluid Flow at Mesoscale Levels (in Chinese), Ph. D. thesis, China University of Mining and Technology, Beijing, 2014
[31] Yang, Y. M., Study on Modeling Porous Structures of Rocks and Mechanical Properties (in Chinese), Ph. D. thesis, China University of Mining and Technology, Beijing, 2008
[32] Blum, H., A Transformation for Extracting New Descriptors of Shape, *Models for the Perception of Speech & Visual Form*, *19* (1967), 5, pp. 362-380
[33] Alraoush, R., *et al.*, Comparison of Network Generation Techniques for Unconsolidated Porous Media, *Soil Sci. Soc. Am. J.*, *67* (2003), 7, pp. 1687-1700

Paper submitted: March 10, 2017
Paper revised: May 1, 2017
Paper accepted: May 22, 2017